Available online at www.sciencedirect.com
ScienceDirect
Catalysis Today 131 (2008) 203–210
CATALYSIS TODAY
www.elsevier.com/locate/cattod

Mesoporous and nanostructured CeO_2 as supports of nano-sized gold catalysts for low-temperature water-gas shift reaction

Zhong-Yong Yuan [a,b,*], Vasko Idakiev [c,*], Aurélien Vantomme [a], Tatyana Tabakova [c], Tie-Zhen Ren [d], Bao-Lian Su [a,*]

[a] *Laboratory of Inorganic Materials Chemistry, The University of Namur (FUNDP), 61 rue de Bruxelles, B-5000 Namur, Belgium*
[b] *Institute of New Catalytic Materials Science, College of Chemistry, Nankai University, Tianjin 300071, PR China*
[c] *Institute of Catalysis, Bulgarian Academy of Sciences, Acad. G. Bonchev Street, bl. 11, 1113 Sofia, Bulgaria*
[d] *Structural Chemistry, Arrhenius Laboratory, Stockholm University, SE-10691 Stockholm, Sweden*

Available online 26 November 2007

Abstract

Mesoporous particles and 1D nanorods of cerium oxides have been prepared by modifying the hydrothermal route of a surfactant-assisted controllable synthesis. Mesoporous cerias were obtained in a sealed glass vessel under continuous stirring, while ceria nanorods were obtained in a Teflon-lined autoclave without stirring. The mesoporous cerias did not show long-range mesoscopic organization, exhibiting a broad mesopore size distribution in the region 8–15 nm. A BET surface area of 100 m^2/g with a total pore volume of 0.33 cm^3/g is obtained for as-synthesized mesoporous ceria. The ceria nanorods exhibit a cubic crystalline structure after calcination, having the lengths in the range of 150–300 nm and diameters in the range of 10–25 nm. The growth direction of ceria nanorods is along [1 1 0]. A surface area of above 50 m^2/g is obtained in the calcined nanorods. These synthesized ceria materials were used as supports of nano-sized gold catalysts, prepared by deposition–precipitation method. Their catalytic activity was evaluated by the low-temperature water-gas shift reaction. The gold/mesoporous ceria catalytic system exhibited higher catalytic activity than gold/ceria nanorods. It is revealed that the mesoporous and nanostructured cerias are of much interest as potential supports for gold-based catalysts that are effective for low-temperature water-gas shift reaction.

Keywords: Cerium oxide; Mesoporous; Nanorods; Gold catalysts; Water-gas shift reaction

1. Introduction

Cerium oxide nanostructures are of considerable importance due to their optical properties, high thermal stability, electrical conductivity and diffusivity, and the ability to store and release oxygen, which have found wide applications such as high-temperature ceramics [1], catalysts [2–4], fuel cells [5–7], silicon-on-insulator structures, barrier layers or capacitor devices. Ceria is a crucial component in the automobile three-way catalysts primarily for its role in oxygen storage, taking up oxygen under oxidising conditions and releasing it under reducing ones [4]. Potential uses of CeO_2 for the removal of soot from diesel engine exhaust, for the removal of organics from wastewaters, as an additive for combustion processes, and in fuel cell technology have been described [8,9]. Gold-supported ceria has been reported as effective catalyst for CO oxidation [10], CH_4 oxidation, catalytic combustion of volatile organic compounds [11], and the low-temperature water-gas shift reaction [12,13].

For the practical applications of ceria, it is desirable to possess a number of specific features such as nano-scaled particle size, crystalline structure, particular morphology, high surface area, and thermal stability. Thus, mesoporous cerium oxides [14–17], macroporous structures [18], nanoparticles [19,20] and films [21], as well as nanorods/nanowires [22–24] have been synthesized, mainly by the chemical methods (the so-called bottom up approach). Chemical methods may provide a more promising route to nanostructures in terms of cost and potential for large-scale production. However, it is still a challenge to control the structure, texture and morphology of cerium oxide nanomaterials. It should be quite significant to

* Corresponding authors.
E-mail addresses: zyyuan@nankai.edu.cn (Z.-Y. Yuan), idakiev@ic.bas.bg (V. Idakiev), bao-lian.su@fundp.ac.be (B.-L. Su).

0920-5861/$ – see front matter © 2007 Elsevier B.V. All rights reserved.
doi:10.1016/j.cattod.2007.10.050

produce nanostructures with well-controlled morphologies and dimensions without the necessity for costly and complex processing.

We have then been able to control the texture, structure and morphology of cerium oxide nanomaterials by modifying the hydrothermal route. Mesoporous structures and 1D nanorods of CeO_2 have controllably been produced. Synthesis was performed by the use of $CeCl_3{\cdot}7H_2O$ as cerium oxide precursor in the presence of surfactant cetyltrimethylammonium bromide (CTMABr). The reaction mixture was aged at 363 K for 90 h either in a sealed glass vessel under continuous stirring or in a Teflon-lined autoclave without stirring. The prepared ceria mesoporous particles and nanorods were further used as supports of nano-sized gold catalysts by deposition–precipitation method. The catalytic activities of gold-supported mesoporous CeO_2 and nanorods were evaluated in low-temperature water-gas shift (WGS) reaction at wide temperature range (140–350 °C), since WGS reaction is one of the key steps involved in automobile exhaust processes, converting CO with water to hydrogen and carbon dioxide, and the hydrogen produced is a very effective reductant for NO_x removal [13,25]. It is shown that these Au/CeO_2 catalysts exhibited very interesting properties for the low-temperature WGS reaction.

2. Experimental

2.1. Preparation of mesoporous CeO_2 and CeO_2 nanorods

$CeCl_3{\cdot}7H_2O$ and CTMABr, received from Aldrich, were used for the synthesis of nanostructured and mesoporous cerium oxide materials. 1.02–9 g CTMABr and 1.25–3.04 g of $CeCl_3{\cdot}7H_2O$ (Ce/surfactant molar ratio of 1.2–0.33) were dissolved in 60 ml of H_2SO_4 aqueous solution (pH 2) at 40 °C under stirring for 1 h, followed by the dropwise addition of 35 ml of ammonia solution (25 wt.%) in 15 min. The pH value of the solution varied from initial value of 2.0 to a final value of 11.4, causing a precipitation and a colour change from colourless to purple. After a further stirring of 1 h, two pathways were followed: (A) the mixture was transferred into a Teflon-lined autoclave, and heated at 80 °C for 4 days under static condition, and then the purple product was filtered and washed with 300 ml of distilled water and dried at 60 °C in an oven, accompanying with a colour change from pale purple to yellow; (B) the mixture was aged at 80 °C for 4 days in a sealed glass vessel under continuous stirring, and a colour change from purple to yellow was observed after 10 h of stirring, and the yellow product was filtered and washed with 300 ml of distilled water and dried at 60 °C in an oven. The sample was then calcined in N_2 for 12 h and in air for 6 h at 550 °C.

2.2. Preparation of supported gold catalysts

Three percent by weight of gold was loaded on the mesoporous cerias and ceria nanorods by deposition–precipitation method. A solution of $HAuCl_4{\cdot}3H_2O$ was used to prepare small particles of supported Au. The gold hydroxide was supported on the prepared CeO_2 samples preliminary suspended in water via the chemical reaction between $HAuCl_4{\cdot}3H_2O$ and Na_2CO_3 in aqueous solution [25]. The samples were dried under vacuum at 80 °C and calcined in air at 400 °C for 2 h. The catalysts were denoted as Au/CeO_2-M and Au/CeO_2-R for the samples supported on mesoporous CeO_2 (CeO_2-M) and CeO_2 nanorods (CeO_2-R), respectively.

2.3. Characterization of samples

X-ray diffraction (XRD) patterns were recorded on a Philips PW 1820 diffractometer with graphite monochromatized Cu Kα radiation (λ = 0.154 nm).

N_2 adsorption–desorption analysis was performed on a Micrometrics Tristar 3000 analyzer at −196 °C. The samples were degassed overnight at 200 °C before analysis. The surface area was calculated by the BET method, and the pore size distribution was determined by the BJH method using the adsorption branch of isotherms.

Scanning electron microscopy (SEM) was performed on a Philips XL-20 microscope at 15 keV, and transmission electron microscopy (TEM) was carried out on a Philips TECNAI-10 microscope at 100 kV. High resolution TEM analysis was performed on a Philips CM30-FEG and a Jeol JEM-3010 microscope at 300 kV.

Fourier transform infrared (FT-IR) spectroscopy was carried out on a Perkin-Elmer Spectrum 2000 spectrometer, and reflectance UV–vis spectroscopy was performed on a Perkin-Elmer I-35 spectrometer.

The gold content in catalysts was analyzed by atomic absorption method.

2.4. Catalytic activity testing

Catalytic activity test was performed in a fixed-bed flow reactor at atmospheric pressure and temperature range from 140 to 350 °C. The following conditions were applied: 0.5 cm^3 of catalyst bed volume, 4000 h^{-1} of space velocity, 31.1 kPa of partial pressure of water vapor, and the reactant gas mixture contained 4.494 vol.% CO in argon. The CO and CO_2 content was analyzed on ''URAS-3G'' and ''URAS-2T'' (Hartmann & Braun AG) gas analyzers and the catalytic activity was expressed by degree of CO conversion.

3. Results and discussion

3.1. Preparation and characterization of mesoporous and nanostructured CeO_2

Fig. 1 shows the XRD patterns of the as-synthesized and calcined CeO_2 samples synthesized with the Ce/surfactant ratios of 1.2 and 0.33 either by static autoclaving or under stirring condition. The diffraction lines of the as-synthesized and calcined samples prepared with low amount of surfactant (*i.e.* Ce/surfactant = 1.2) by static autoclaving are similar in the 2θ range of 10–80°, which could be indexed to (1 1 1), (2 0 0), (2 2 0), (3 1 1), (4 0 0), (3 3 1) and (4 2 0) corresponding to a fluorite-structured ceria phase [space group: *Fm*3*m*] (JCPDS

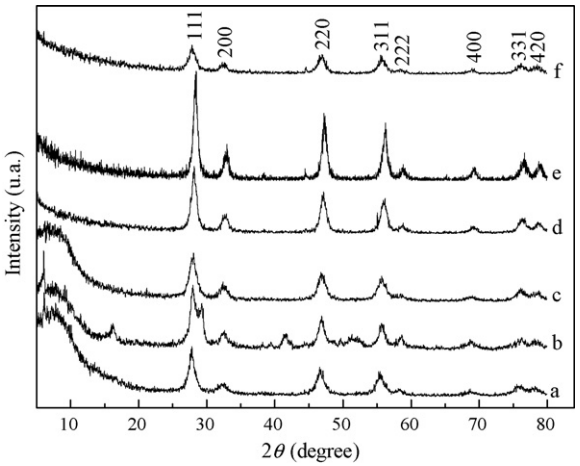

Fig. 1. X-ray diffraction patterns of the as-synthesized CeO_2 samples obtained by static autoclaving with Ce/surfactant molar ratios of (a) 1.2 and (b) 0.33, and obtained (c) under stirring condition with Ce/surfactant ratio of 1.2. (d–f) are the calcination forms of (a–c), respectively.

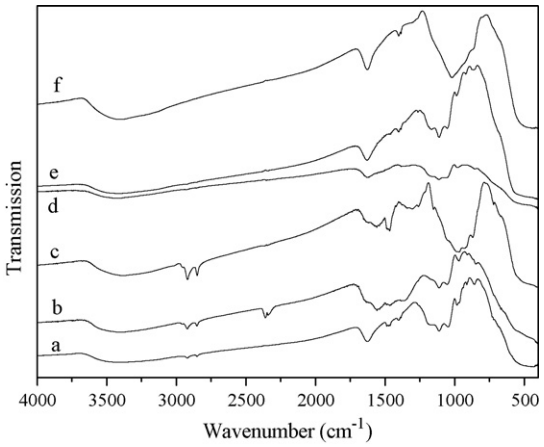

Fig. 2. FT-IR spectra of the as-synthesized CeO_2 samples obtained by static autoclaving with Ce/surfactant molar ratios of (a) 1.2 and (b) 0.33, and obtained (c) under stirring condition with Ce/surfactant ratio of 1.2. (d–f) are the calcination forms of (a–c), respectively.

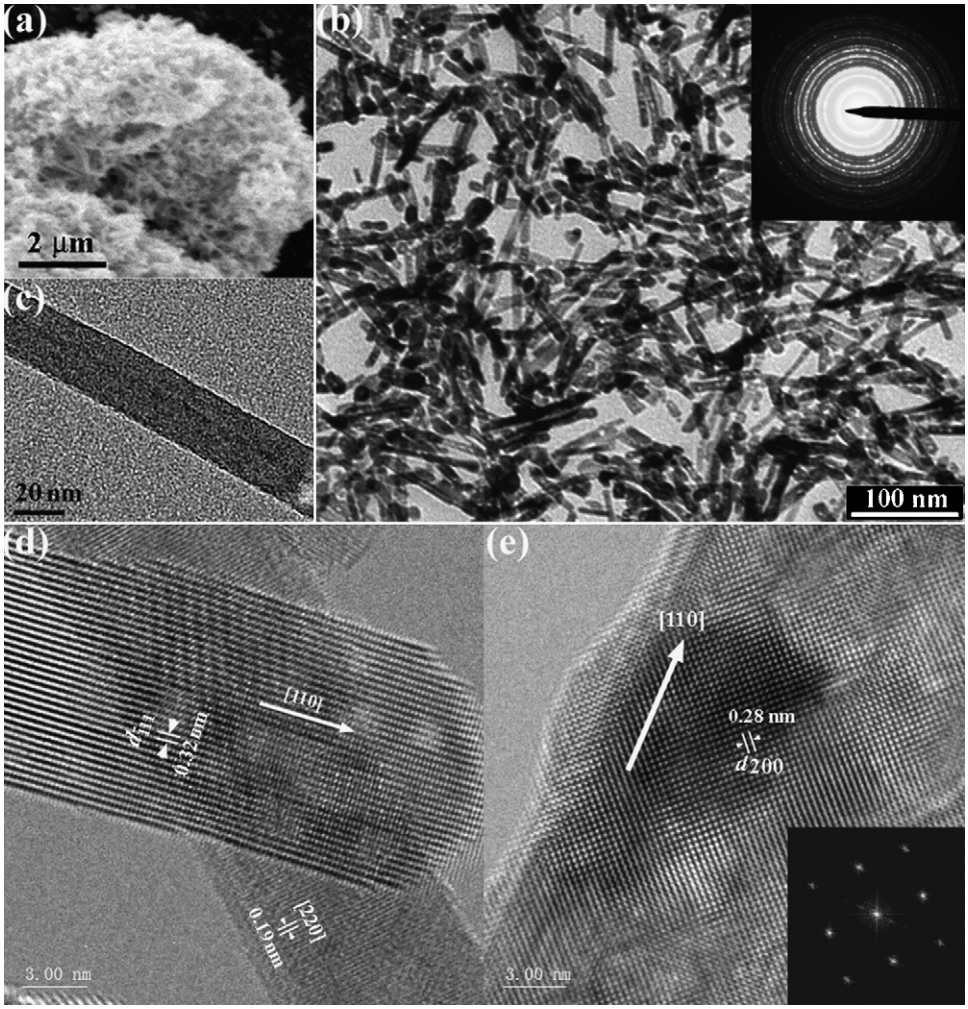

Fig. 3. (a) SEM image of an aggregation of ceria nanorods; (b) low-magnification TEM image of ceria nanorods, giving an overview of large-scale nanorods, and electron diffraction pattern (inset); (c) TEM image of one single nanorod; (d) HRTEM image of two crossed nanorods; (e) HRTEM image of one nanorod recorded along the $[\bar{1}\,1\,1]$-zone-axis and its FFT pattern (inset).

34-0394) with lattice constant a of 0.549 and 0.548 nm, respectively (Fig. 1a and d). Whilst, the as-synthesized sample prepared with large amount of surfactant (Ce/surfactant = 0.33) by static autoclaving presents two sets of diffraction lines (Fig. 1b): one set of diffraction peaks can be indexed well to a pure cubic CeO_2 structure ($a = 0.542$ nm), and the other weakly diffraction lines are attributed to the hexagonal structure of $Ce(OH)_3$ [space group: $P6_3/m$] with lattice constants $a = 0.635$ nm and $c = 0.365$ nm (JCPDS 19-0284). After calcination at 550 °C to remove the surfactant species, a pure cubic CeO_2 structure ($a = 0.547$ nm) is obtained due to the conversion of $Ce(OH)_3$ to CeO_2 (Fig. 1e). For the CeO_2 samples synthesized under the stirring condition, both the as-synthesized and calcined samples exhibit diffraction lines assignable to the cubic fluorite structure of ceria (Fig. 1c and f). The cell parameters (a) of the as-synthesized and calcined samples are 0.547 and 0.548 nm, respectively. The crystallite sizes of the resultant CeO_2 synthesized with Ce/surfactant of 1.2 and 0.33 by static autoclaving, and synthesized with Ce/surfactant of 1.2 under stirring condition, calculated by the Scherrer formula from the (1 1 1) peak of the calcined samples, are about 8.9, 11.4 and 6.4 nm, respectively.

All the patterns of the as-synthesized samples exhibit one peak at low angle $2\theta = 6^\circ$, resulting from the interaction between surfactant molecules and ceria species, which is confirmed by the FT-IR spectra (Fig. 2). As shown in Fig. 2a–c, the spectra of the as-synthesized samples exhibit absorption bands in the region of 2800–2900 cm^{-1}, attributed to the C–H stretching mode of hydrocarbons, and the bands at 1450–1500 and 720 cm^{-1}, assigned to the bending vibration of the C–H band of methylene groups of the surfactant alkyl chain. These bands should be consistent with the diffraction line of $2\theta = 6^\circ$, suggestive of the participated surfactant species, which disappear after calcination.

The porosity and morphology are the important features for the applications in many fields. In the present work, it is found that the morphology of the resultant cerium oxide materials could be affected by the ageing process of the reaction mixtures and the surfactant/Ce molar ratios. The static autoclaving at 80 °C of the synthesis gel with high surfactant/Ce ratio resulted in the formation of cerium oxide nanorods, while the ageing under stirring condition with low surfactant/Ce ratio lead to the formation of mesoporous cerium oxide particles.

Fig. 3 shows the SEM and low-magnification TEM images of the cerium oxide materials synthesized by the static autoclaving with the ceria/surfactant ratio of 0.33. A large quantity of nanorods are clearly seen, which aggregated in a scaffold-like array into congeries of tens to several tens micrometers in size with large interparticular porosity. The diameters of the nanorods are in the range of 10–25 nm, and the lengths in the range of 150–300 nm. The cross-sectional TEM images also reveal that the nanorods do not have a perfect circular cross section perpendicular to its axis, but a polygon, which is characteristic of well-crystalline nanostructures. However, the content of nanorods decreased with the surfactant content in the synthesis, and the granular nanoparticle aggregates instead. For example, the yield of nanorods decreased from 80% to 30% when the Ce/surfactant ratio increased from 0.33 to 1.2. Almost no rod-like particles were observed when the synthesis was performed in the absence of surfactant CTMABr.

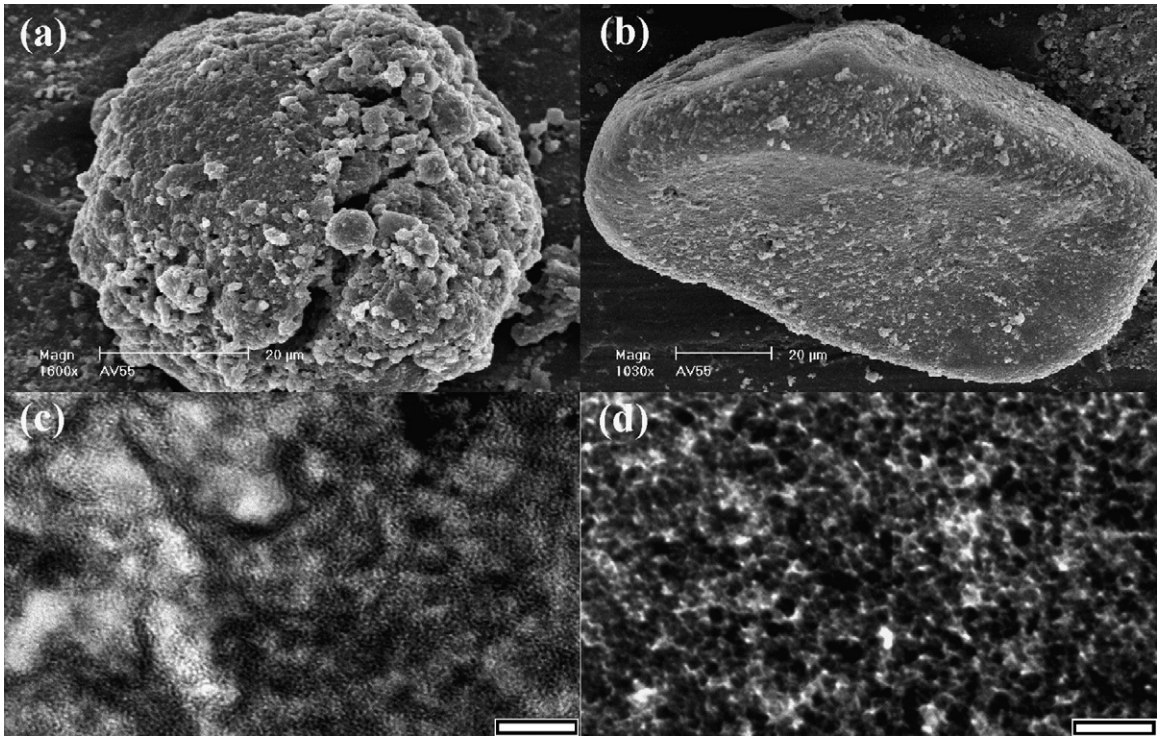

Fig. 4. (a and b) SEM and (c and d) cross-sectional TEM images of the mesoporous ceria synthesized under stirring condition. Scale bar of 20 μm in (a and b), and 50 nm in (c and d).

The crystalline nature of the resultant CeO_2 nanorods can be verified by the electron diffraction patterns (Fig. 3b). Fig. 3d and e displays the high resolution TEM (HRTEM) images of the calcined CeO_2 nanorods synthesized with Ce/surfactant molar ratio of 0.33, showing that the nanorods are structurally uniform and single crystalline with [1 1 0] growth direction. The lattice fringe spacings are consistent with those of bulk CeO_2. The HRTEM image of Fig. 3e is recorded with electron beam parallel to the $[\bar{1}\,1\,1]$ axis, reflected from the lattice fringes and the corresponding Fast Fourier Transform (FFT) pattern.

Fig. 4a and b is the typical SEM micrographs of the as-synthesized and calcined samples synthesized by ageing under the stirring condition. The samples have typical features of an agglomeration of small sized particles with irregular shapes. Their cross-sectional TEM images (Fig. 4c and d) show that the particles are of mesoporous structure with disorder wormhole-like interconnected channels, formed by the agglomeration of ceria nanoparticles.

The N_2 adsorption–desorption isotherms of the CeO_2 nanorods synthesized by static stirring are of type II (Fig. 5), indicating multi-layer adsorption on flat surfaces of the nanorods. The hysteresis loop at high relative pressures is the result from the interparticulate spaces in the scaffold-like assembly of nanorods. The BET surface areas of 114 m^2/g (Ce/surfactant = 1.2) and 100 m^2/g (Ce/surfactant. = 0.33) are obtained from the uncalcined materials with very large pore volumes of 0.934 and 0.863 cm^3/g, respectively. Calcination results in the significant decrease of the surface area to 74 and 54 m^2/g, and pore volume to 0.529 and 0.515 cm^3/g, respectively.

Fig. 6 depicts the nitrogen adsorption–desorption isotherms and corresponding pore size distribution of the samples prepared with Ce/surfactant = 1.2 under stirring condition. Similar type IV isotherms with hysteresis loops of type H2 are obtained for the both as-synthesized and calcined samples, confirming the obvious mesoporous structure, which has been observed by TEM. A high BET surface area of 100 m^2/g is obtained from the uncalcined sample with a low pore volume of 0.343 cm^3/g. After calcination, the surface area and pore volume of the mesoporous ceria decrease slightly to 72 m^2/g and 0.269 cm^3/g. The pore size distribution of the uncalcined sample covers the range 5–20 nm, with a maximum at around 10 nm.

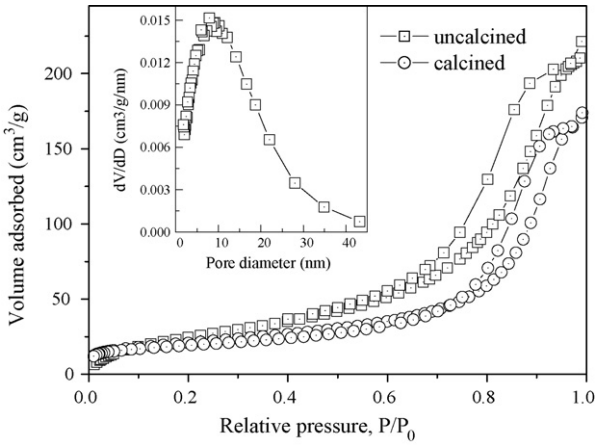

Fig. 6. N_2 adsorption–desorption isotherms of the as-synthesized and calcined mesoporous cerias obtained with Ce/surfactant = 1.2 under stirring conditions. Inset is the BJH pore size distribution curve of the as-synthesized sample obtained from the adsorption branch of the isotherms.

3.2. Structural, textural and catalytic properties of Au/CeO_2 catalysts

The XRD patterns of the Au/CeO_2 catalyst samples are shown in Fig. 7. Fig. 8 lists the enlarged patterns at 2θ range of 35–45° in order to show the diffraction lines of gold particles. Compared with the diffraction lines of pure mesoporous CeO_2 and nanorods shown in Fig. 1, the catalysts Au/CeO_2-R and Au/CeO_2-M show weak diffraction lines of gold at $2\theta = 38.2°$ and 44.4°, besides the fluorite phase of CeO_2. The average sizes of gold particles in Au/CeO_2-R and Au/CeO_2-M, determined from XRD line broadening of (1 1 1) by the Scherrer equation, are 11.1 and 6.3 nm, respectively.

TEM observation revealed that the gold nanoparticles are homogeneously dispersed on the both metal oxide supports.

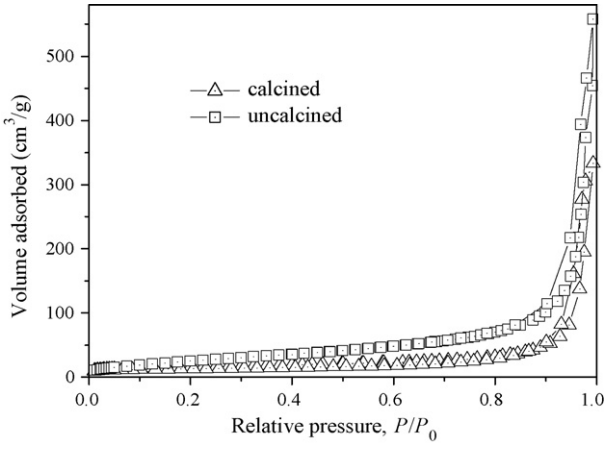

Fig. 5. N_2 adsorption–desorption isotherms of the as-synthesized and calcined ceria nanorods obtained with Ce/surfactant = 0.33 by static autoclaving.

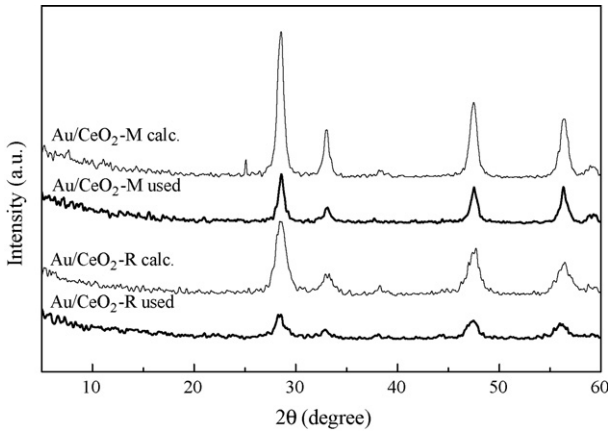

Fig. 7. X-ray diffraction patterns of the gold-based catalysts calcined at 400 °C and after catalytic testing (used).

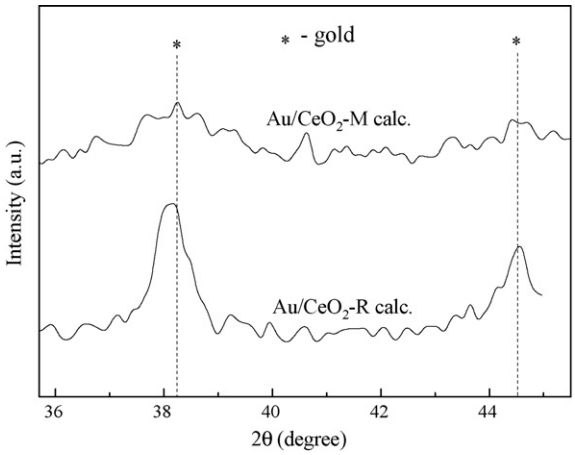

Fig. 8. X-ray diffraction patterns of the catalysts calcined at 400 °C in the angle interval of 35–45° (2θ).

The particle size distributions of gold in these two catalysts are in nanometer scale, which is consistent with the XRD analysis results. The gold particle size distribution of Au/CeO_2-M is relatively narrow, mainly in the range of 5–7 nm (Fig. 9). However, the gold particle size distribution of Au/CeO_2-R is relatively broad, in the range of 5–30 nm, though mainly in the range of 5–15 nm (Fig. 10). Small quantity of gold particles with large size (even 30 nm) can be observed (Fig. 10b). The supported Au nanoparticles in both Au/CeO_2-M and Au/CeO_2-R catalysts are most probably polycrystalline, as revealed by the electron diffraction. The smaller particle size of gold in Au/CeO_2-M than in Au/CeO_2-R suggests that the mesoporous structure of the support may be more suitable for the formation and dispersion of nano-sized gold particles. The mesoporous CeO_2 supplied the high-surface area and narrow pore size distribution, benefiting the finely dispersion of gold nanoparticles.

The catalytic activity of the Au/CeO_2-R and Au/CeO_2-M catalysts in low-temperature WGS reaction, measured in the temperature range 140–350 °C, is presented in Fig. 11. The activity of pure ceria in the WGS reaction becomes significant only at temperatures above 300 °C [26]. While the Au/CeO_2 catalysts, whatever the structural type of the supports, exhibit the interesting catalytic activity at low-temperatures. As seen from Fig. 11, Au/CeO_2-M exhibits the higher CO conversion than Au/CeO_2-R. At the high temperature range, the activity of Au/CeO_2-M is comparable with that of the reference catalyst Au/CeO_2 [13] with the same gold content. However, the activity of Au/CeO_2-M is higher than that of reference catalyst when the reaction was performed at low temperatures. The catalytic activity seems to be somewhat consistence with the gold

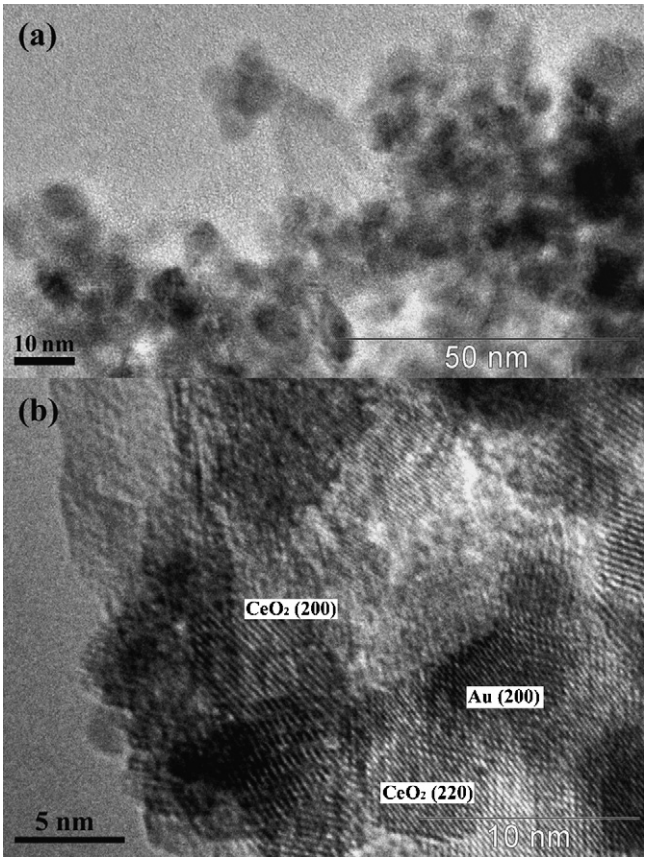

Fig. 9. HRTEM images of Au/CeO_2-M catalyst calcined at 400 °C.

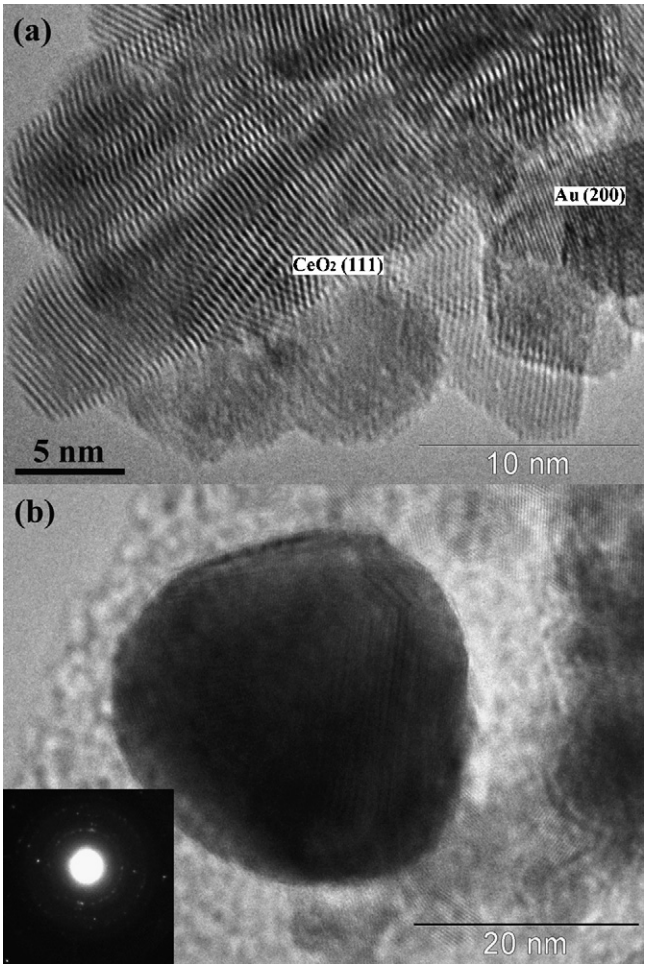

Fig. 10. HRTEM images of Au/CeO_2-R catalyst calcined at 400 °C. (b) Shows one gold particle with a little large size, and the corresponding electron diffraction pattern (inset).

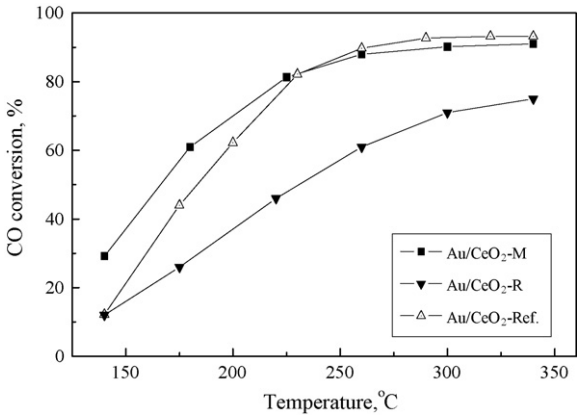

Fig. 11. WGS activity of gold catalysts supported on CeO_2-M and CeO_2-R, compared to the reference Au/CeO_2 catalyst [13].

particle size in Au/CeO_2 catalysts. Smaller gold particles in catalysts show the higher catalytic activity of WGS reaction. The average size of gold particles in reference Au/CeO_2 catalyst is about 5.5 nm, which is comparable with that in Au/CeO_2-M (∼6 nm) and smaller than that in Au/CeO_2-R sample (∼11 nm). Correspondingly, the catalytic activity of reference Au/CeO_2 catalyst is comparable with that of Au/CeO_2-M, and higher than that of Au/CeO_2-R. It has been known that the catalytic activity and selectivity is controlled by the contact structure of Au nanoparticles with the support, the selection of support materials, and the size of Au particles [25,27]. The role of perimeter interface between Au particles and the support is emphasized as a unique reaction site for the reactants [28]. The specific interaction on the border between gold and the support could also play an important role [29]. New reaction sites appear at the metal-support perimeter interface with a decrease in the size of gold particles. When mesoporous CeO_2 was used as support, the size of gold particles is smaller, this may lead to the increase of the fractions of the active sites (e.g. edge, corner or step sites), resulting in the increase in catalytic activity. Thus, the contact structure being the most important because the perimeter interfaces around Au particles and ceria surfaces act as the sites for reaction. In our previous reports on the mesoporous metal oxides as supports [25,27], it has been revealed that the WGS activities of the supported gold catalysts correlate with the particle sizes of gold, rather than the content of gold loading, in spite of the different nature of the supports. This effect is related to the contact structure between Au nanoparticles and the support.

4. Conclusions

A surfactant-assisted controllable hydrothermal synthesis route has been successfully developed to the preparation of 1D nanorods and mesoporous cerium oxides. It is found that the surfactant concentration and the stirring during the hydrothermal treatment are key factors to influence the final cerium oxide structures. After calcination, the nanorods present a fluorite single-crystalline structure with lengths in the range of 150–300 nm and diameters ranging from 10 to 25 nm. The mesoporous ceria particles present a high surface area (100 m^2/g in as-synthesized form) and disordered mesopores with pore size in the range of 8–15 nm. These new ceria structures can be used as potential supports for nano-sized gold-based catalysts. The catalytic activity of Au/CeO_2-M in low-temperature WGS reaction is higher than that of Au/CeO_2-R. The high and stable WGS activity could be related to the high stability of nano-sized gold dispersion and to larger number of active sites located at the Au/mesoporous ceria interface. The prepared mesoporous and nanostructured Au/ceria catalyst systems may be of interest in the other catalytic applications.

Acknowledgements

This work was financially supported by the European Program of InterReg III (Programme France-Wallonie-Flandre, FW-2.1.5), and realised in the frame of the Belgian Federal Government PAI-IUAP-01/5 project. Z.-Y. Yuan thanks the supports of the National Natural Science Foundation of China (No. 20473041 and 20673060) and the National Basic Research Program of China (No. 2003CB615801). V. Idakiev and T. Tabakova thank the National Science Fund of Bulgaria (project 2K-11) and the Joint Research Project between the CGRI in Belgium and Bulgarian Academy of Sciences. A. Vantomme thanks Fonds National de la Recherche Scientifique (FNRS, Belgium) for a FRIA scholarship.

References

[1] K. Eguchi, J. Alloys Compd. 250 (1997) 486.
[2] T. Inoue, M. Osonoe, H. Tohda, M. Hiramatsu, J. Appl. Phys. 69 (1991) 8313.
[3] B.E. Park, I. Sakai, E. Sakai, E. Tokumitsu, H. Ishiwara, Appl. Surf. Sci. 117/118 (1997) 423.
[4] A. Trovarelli, Catal. Rev. Sci. Eng. 38 (1996) 439.
[5] H. Inaba, H. Tagawa, Solid State Ionics 83 (1996) 1.
[6] B.C.H. Steele, Solid State Ionics 129 (2000) 95.
[7] E.P. Murray, T. Tsai, S.A. Barnett, Nature 400 (1999) 649.
[8] A. Trovarelli, C. de Leitenburg, M. Boaro, G. Dolcetti, Catal. Today 50 (1999) 353.
[9] Y. Li, Q. Fu, M. Flytzani-Stephanopoulos, Appl. Catal. B: Environ. 27 (2000) 179.
[10] U.R. Pillai, S. Deevi, Appl. Catal. A 299 (2006) 266.
[11] S. Scire, S. Minico, C. Crisafulli, C. Satriano, A. Pistone, Appl. Catal. B: Environ. 40 (2003) 43.
[12] Q. Fu, A. Weber, M. Flytzani-Stephanopoulos, Catal. Lett. 77 (2001) 87.
[13] D. Andreeva, V. Idakiev, T. Tabakova, L. Ilieva, P. Falaras, A. Bourlinos, A. Travlos, Catal. Today 72 (2002) 51.
[14] A. Corma, P. Atienzar, H. Garcia, J.Y. Chane-Ching, Nat. Mater. 3 (2004) 394.
[15] D. Terribile, A. Trovarelli, J. Llorca, C. de Leitenburg, G. Dolcetti, J. Catal. 178 (1998) 299.
[16] D.M. Lyons, K.M. Ryan, M.A. Morris, J. Mater. Chem. 12 (2002) 1207.
[17] S.C. Laha, R. Ryoo, Chem. Commun. (2003) 2138.
[18] A. Bouchara, G.J.A.A. Soler-Illia, J.Y. Chane-Ching, C. Sanchez, Chem. Commun. (2002) 1234.
[19] W. Bai, K.L. Choy, N.H.J. Stelzer, J. Schoonman, Solid State Ionics 116 (1999) 225.
[20] D.S. Bae, B. Lim, B.I. Kim, K.S. Han, Mater. Lett. 56 (2002) 610.
[21] M. Lundberg, B. Skarman, F. Cesar, L.R. Wallenberg, Microporous Mesoporous Mater. 54 (2002) 97.
[22] C. Sun, H. Li, Z.X. Wang, L. Chen, X. Huang, Chem. Lett. 33 (2004) 662.

[23] M. Yada, S. Sakai, T. Torikai, T. Watari, S. Furuta, H. Katsuki, Adv. Mater. 16 (2004) 1222.
[24] A. Vantomme, Z.Y. Yuan, G. Du, B.L. Su, Langmuir 21 (2005) 1132.
[25] V. Idakiev, T. Tabakova, Z.Y. Yuan, B.L. Su, Appl. Catal. A 270 (2004) 135.
[26] B.I. Whittington, C.J. Jiang, D.L. Trimm, Catal. Today 26 (1995) 41.
[27] V. Idakiev, T. Tabakova, A. Naydenov, Z.Y. Yuan, B.L. Su, Appl. Catal. B 63 (2006) 178.
[28] M. Haruta, M. Date, Appl. Catal. A 222 (2001) 427.
[29] V. Idakiev, Z.Y. Yuan, T. Tabakova, B.L. Su, Appl. Catal. A 281 (2005) 149.